Multi-Frequency Pierce Oscillators Based On Piezoelectric AlN Contour-Mode MEMS Resonators

Chengjie Zuo[1], Nipun Sinha[2], Jan Van der Spiegel[1], and Gianluca Piazza[1,2]
[1]Department of Electrical and Systems Engineering
[2]Department of Mechanical Engineering and Applied Mechanics
University of Pennsylvania, Philadelphia, PA 19104, USA
{czuo, nipun, jan, piazza}@seas.upenn.edu

***Abstract* — This paper reports on the first demonstration of multi-frequency (176, 222, 307, and 482 MHz) oscillators based on piezoelectric AlN contour-mode MEMS resonators. All the oscillators show phase noise values between –88 and –68 dBc/Hz at 1 kHz offset and phase noise floors as low as –160 dBc/Hz at 1 MHz offset. The same Pierce circuit design is employed to sustain oscillations at the 4 different frequencies, while the oscillator core consumes at most 10 mW. The AlN resonators are currently wirebonded to the integrated circuit realized in the AMIS 0.5 µm 5 V CMOS process. This work constitutes a substantial step forward towards the demonstration of a single-chip multi-frequency reconfigurable timing solution that could be used in wireless communications and sensing applications.**

***Keywords* — Pierce Oscillator, Multi-Frequency Oscillator, AlN Contour-Mode Resonator, MicroElectroMechanical Systems (MEMS), Piezoelectric Resonator**

I. INTRODUCTION

Timing is crucial for almost all electronic applications. Data computation and communication generally require a reference signal or source to enable system synchronization and signal modulation. The key part of a reference source is an oscillator circuit that produces a stable output signal with a well-defined frequency spectrum without the need for an input signal. An oscillator can be treated as a positive-feedback amplifier that keeps amplifying noises in the circuit or the power supply until nonlinearities occur and a stable oscillation builds up. The high precision and purity of the signal frequency is usually achieved by placing a high-*Q* resonator in the passive feedback network. For example, quartz crystal, Surface Acoustic Wave (SAW), and Film Bulk Acoustic Resonators (FBAR) have been widely used.

Although few electronic components have stood the test of time better than quartz crystal resonators and oscillators, MicroElectroMechanical Systems (MEMS) technology has emerged as a very promising and competitive alternative due to its small form-factor, high operating frequency up to GHz, and especially the possibility to be fully integrated with Integrated Circuits (IC) to form a single-chip multi-band reconfigurable Radio Frequency (RF) solution for next-generation wireless communications. Large scale MEMS-IC co-integration will not only lead to reduction in fabrication cost, routing parasitics and power consumption, but also open the possibility for completely new RF architectures and even electromechanical-based computing.

For reference oscillator applications, significant work has been done to develop MEMS resonator technologies based on electrostatic [1] and piezoelectric [2] transduction mechanisms that are capable of providing multiple frequencies of operation on a single chip. Among them, the aluminum nitride (AlN) contour-mode RF MEMS technology [3] stands out as the only technology that can reliably span a wide frequency range from 10 MHz up to several GHz, and simultaneously offer high *Q* in air (1,000 – 4,000) and low motional resistance (25 – 1000 Ω), which makes the devices easily interfaced to conventional electronics without the need for special circuit design or complicated matching networks. It has also been demonstrated that piezoelectric RF MEMS switches [4] can be monolithically integrated with AlN contour-mode resonators on the same silicon substrate. By using a seven-mask post-CMOS compatible micro-fabrication process, switches can be co-fabricated with AlN resonators and used to turn on and off different frequency resonators on the same silicon die. In this work, we will continue to show the advantages of this new technology by presenting the first ever demonstration of multi-frequency (176, 222, 307, and 482 MHz) oscillators based on piezoelectric AlN contour-mode resonators. All the oscillators show Phase Noise (*PN*) values between –88 and –68 dBc/Hz at 1 kHz offset and *PN* floor values as low as –160 dBc/Hz at 1 MHz offset. The same Pierce circuit design is employed to sustain oscillations at the 4 different frequencies. As shown in Fig. 1, the resonator is wirebonded to the IC chip. In all cases the oscillator core consumes a low power of 10 mW in the AMIS 0.5 µm 5 V CMOS process.

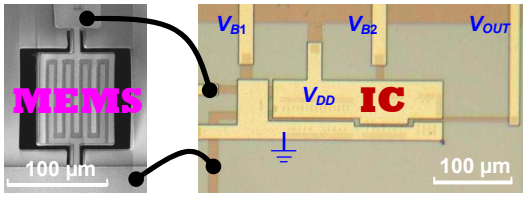

Fig. 1. Micrograph of the Pierce oscillator circuit and its wirebonding with a 482 MHz piezoelectric AlN contour-mode MEMS resonator.

II. PIEZOELECTRIC ALN CONTOUR-MODE RESONATOR

The operating principle of piezoelectric AlN contour-mode resonators has been introduced in previous papers [2, 5]. The one-port higher-order resonator that we used in our oscillator design consists of a 2 μm AlN film sandwiched between two Platinum (Pt) film layers. The bottom and top Pt electrodes are patterned and connected to the electrical signal or ground lines in an alternating way (Fig. 2) such that a higher order contour-mode vibration is selectively excited in the piezoelectric AlN rectangular plate [5]. The resonant frequency is primarily set by the finger (sub-resonator) width, W (Fig. 2), which can be accurately designed at the CAD level and set by the photolithography process. As a one-port electromechanical device, the electrical behavior can be represented by an equivalent circuit called the Modified Butterworth-Van Dyke (MBVD) model [6]. The finite-Q mechanical resonance is described by the motional branch C_M, L_M, and R_M; the electrical capacitance and loss existing in the piezoelectric transducer and substrate parasitics are all lumped into C_0 and R_0; finally, R_S is used to account for the resistance of the routing pads and electrodes.

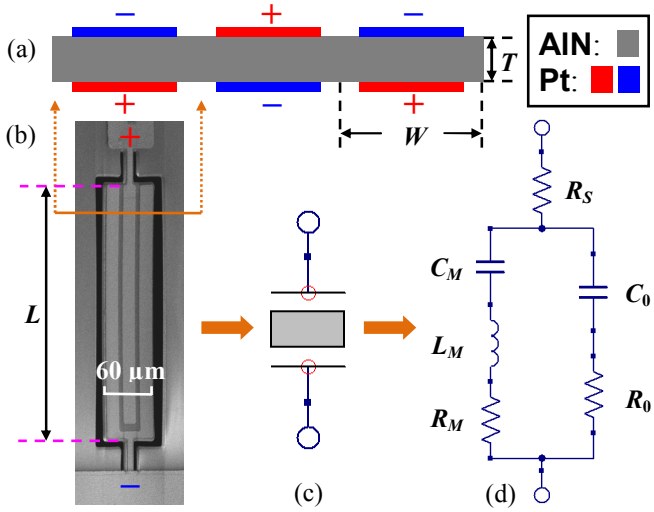

Fig. 2. (a) Cross-sectional schematic, (b) SEM picture, (c) circuit symbol, and (d) MBVD equivalent circuit of a piezoelectric AlN contour-mode resonator.

The measured admittance plot (magnitude and phase), the MBVD model fitting curve, and the corresponding equivalent circuit parameters of a piezoelectric AlN contour-mode resonator operating at 222 MHz are given in Fig. 3. The listed f_s, Q_s, f_p, and Q_p indicate the extracted resonant frequencies and quality factors at series and parallel resonances, respectively. k_t^2 is the extracted effective electromechanical coupling coefficient [2]. As we can see, the device admittance is mainly capacitive and dominated by C_0, but for frequencies between f_s and f_p the resonator behaves like an inductor. Since all available amplifiers are capacitive, the resonator has to operate in the inductive region for oscillation to happen according to the Barkhausen criterion [7]. To serve as an effective inductor in the oscillator circuit, the resonator should be designed so that the phase of its admittance (Fig. 3) is as close to –90° as possible in the inductive region. On the other hand, for better purity of the oscillating frequency, we should design the sustaining circuit so that the oscillator operates as close as possible to the series resonant frequency f_s, because this is the frequency primarily set by the intrinsic electromechanical behavior of the piezoelectric structure and also least dependent on parasitic capacitances coming from the silicon substrate, bonding pads or packaging.

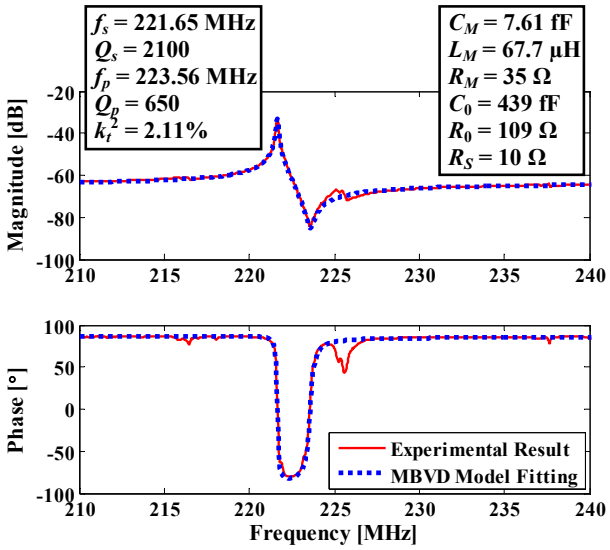

Fig. 3. Measured admittance plot and its MBVD model fitting of a piezoelectric AlN contour-mode resonator at 222 MHz.

With geometry and equivalent circuit parameters known, the resonator can be further characterized by a physical model, as expressed by the following equations [5]:

$$C_0 \approx n\varepsilon_{33}\varepsilon_0 \frac{WL}{T}, \qquad R_M = \frac{1}{n}\frac{\pi}{8}\frac{T}{L}\frac{\rho_{eq}^{1/2}}{E_{eq}^{3/2} d_{31}^2 Q_{su}},$$

$$C_M = n\frac{8}{\pi^2}\frac{WL}{T}E_{eq}d_{31}^2, \qquad L_M = \frac{1}{n}\frac{\rho_{eq}}{8}\frac{WT}{L}\frac{1}{E_{eq}^2 d_{31}^2},$$

$$\omega_s = 2\pi f_s = \frac{\pi}{W}\sqrt{\frac{E_{eq}}{\rho_{eq}}} \qquad (1)$$

where ε_0 is the permittivity of free space, ε_{33} is the dielectric constant of AlN along the c-axis; L, W and T refer to the length, width and thickness of the sub-resonator respectively; n is the number of sub-resonators (fingers); E_{eq} and ρ_{eq} are the equivalent in-plane modulus of elasticity and mass density of AlN and the stacked electrodes; d_{31} is the (3, 1) entry in the AlN's d-form piezoelectric coefficient matrix; ω_s is the series resonant frequency and Q_{su} is the unloaded quality factor at series resonance. The final fitting parameters for the 222 MHz resonator are listed in Table I.

Table I. Physical fitting parameters of the 222 MHz resonator.

ρ_{eq}	5076 kg/m^3	W	20 μm
E_{eq}	399 GPa	L	200 μm
ε_{33}	9	T	2 μm
Q_{su}	2700	n	3
R_S	10 Ω	d_{31}	-1.98 pCN^{-1}
R_0	109 Ω	ε_0	8.85×10^{-12} F/m

III. PIERCE CIRCUIT DESIGN

The simplest amplifier in CMOS technology is a single NMOS transistor. If we connect a resonator between the Drain and Gate of the transistor, a feed-back path is created from the output (Drain) to the input (Gate) of the amplifier, which forms a basic three-point oscillator [7]. Depending on which node is grounded, three variations of the circuit can be constructed, called 'Pierce', 'Colpitts' and 'Santos' oscillator circuits. The Pierce circuit is the one with grounded Source configuration (Fig. 4) and it is also the most used topology for quartz crystal oscillators due to its excellent performance in stability and reliability [8, 9]. Since piezoelectric AlN contour-mode resonators can be considered as MEMS counterparts of quartz crystal Bulk Acoustic Wave (BAW) resonators, the Pierce circuit certainly becomes a very good candidate for the demonstration of our multi-frequency oscillators based on the AlN contour-mode RF MEMS technology.

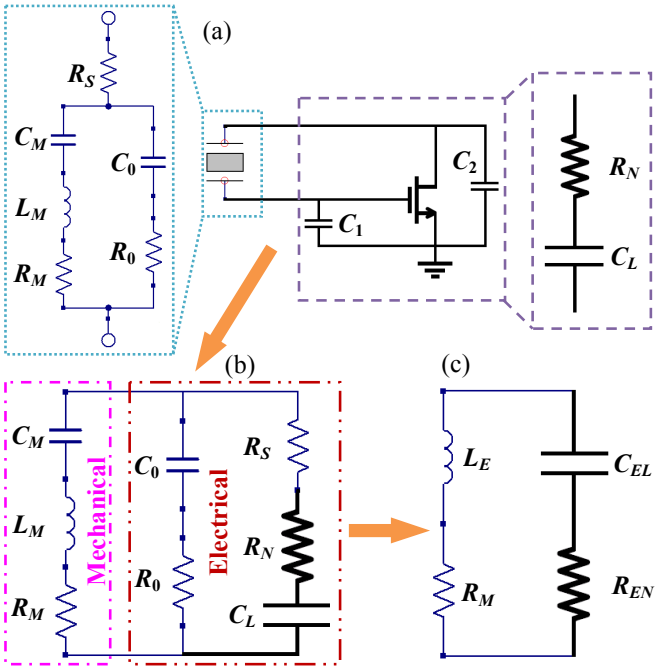

Fig. 4. (a) Equivalent circuits of the Pierce oscillator operating near the oscillation frequency. (b) Separation of the motional (mechanical) and electrical parts of the circuit. (c) Rearrangement to simplify the analysis.

The Vittoz method [8] has been commonly used for the small-signal analysis of three-point oscillators with crystal resonators. However, since electrode and substrate parasitics (e.g., R_S and R_0 in Fig. 2) play a significant role in device performances at the microscale [10], the Vittoz method should be modified accordingly for the design of oscillators based on MEMS resonators. As shown in Fig. 4 (a), the active branch of the Pierce oscillator can be considered equivalent to a negative resistance R_N in series with a load capacitance C_L, the values of which are given as follows:

$$R_N = -\frac{g_m}{\omega^2 C_1 C_2}, \quad C_L = \frac{C_1 C_2}{C_1 + C_2} \tag{2}$$

where ω (=$2\pi f$) is the operating frequency, g_m is the small-signal transconductance of the NMOS transistor, C_1 and C_2 are respectively the Gate-Source and Drain-Source capacitances. If we separate the motional (mechanical) part of the MBVD model from the other part of the equivalent circuit as in Fig. 4 (b), and with some mathematical manipulation, the Pierce circuit operating near the oscillation frequency f_o can be finally simplified to a four-component network that consists of an effective inductance L_E, an effective load capacitance C_{EL}, an effective negative resistance R_{EN}, and the motional resistance, R_M, of the resonator, as shown in Fig. 4 (c). The effective values can be derived as:

$$L_E \approx \frac{2(\omega-\omega_s)}{\omega^2\omega_s C_M} = \frac{2p}{\omega^2 C_M}, \quad p = \frac{\omega-\omega_s}{\omega_s} << 1$$

$$Z_{ET} = \left[R_N + R_S + 1/(j\omega C_L)\right] \| \left[R_0 + 1/(j\omega C_0)\right]$$

$$R_{EN} = \text{real}\{Z_{ET}\}, \quad C_{EL} = -1/\left[\omega \cdot \text{imag}\{Z_{ET}\}\right] \tag{3}$$

where p is defined to be the frequency pulling factor which indicates the relative amount of frequency pulling above the series resonant frequency ω_s (=$2\pi f_s$) of the resonator [7], Z_{ET} is the total impedance of the electrical part in Fig. 4 (b), '||' means parallel electrical connection, and 'real' and 'imag' denote real and imaginary parts of a complex number, respectively. By equating R_{EN} with $-R_M$ and solving Equation (3), the critical transconductance g_{mc} and operating frequency ω_c for starting oscillations can be estimated.

Using the analytical models for the resonator and circuit, we performed power optimization for the design of a single Pierce circuit that works for all resonators at different frequencies. First of all, it has been shown by Vittoz [8] that g_{mc} reaches a minimum when C_1 is equal to C_2. Further, Sansen [7] indicates that a large absolute value of C_1 (= C_2) will require a large bias current and consequently large static power to sustain the oscillation. Therefore, to minimize static power consumption of the Pierce oscillators, no external capacitors were added for C_1 or C_2 in our design based on piezoelectric AlN contour-mode MEMS resonators, and the parasitic capacitances from the transistors, interconnects and bonding pads were instead utilized. As a worst case estimation, we assumed $C_1 = C_2 = 1$ pF in our analysis.

In Fig. 5 – 7, the critical transconductance g_{mc} is plotted as a function of Q_s, k_t^2, nL, T, f, and R_0, while all other parameters are kept fixed. From Fig. 4 (c), we can see that the primary power loss in the oscillator is due to the motional resistance R_M of the resonator. R_M is inversely proportional to $Q_s \cdot k_t^2$, which is defined to be the Figure of Merit (FoM) of a resonator. For the piezoelectric AlN contour-mode MEMS technology, the maximum achievable k_t^2 is limited to ~3% theoretically. Therefore, in order to reduce g_{mc}, and thus the biasing current and static power consumption, we can act on the resonator Q and try to make it as high as possible (Fig. 5). At the same time, a high Q is also very critical in obtaining good phase noise performance of the final oscillator. In our case, the demonstrated Q_s are limited between 1,000 and 3,000 in air. They are sufficient to demonstrate good performance oscillators and guarantee low power consumption, but further improvements in device Q can clearly enhance the overall

oscillator performances in terms of power consumption and phase noise.

With a fixed transduction mechanism, we can then act on the device geometry in order to minimize g_{mc}. Since the resonator width, W (Fig. 2), is used to define the resonant frequency in the piezoelectric AlN contour-mode technology, only the length L and thickness T are available to minimize g_{mc}. Higher-order resonators can be considered as multiple sub-resonators electrically connected in parallel. Therefore we should use the effective length, nL, (which is the number of fingers multiplied by the actual length of each sub-resonator). In this way, we can effectively control the layout geometry by acting on both L and n. As shown in Fig. 6, the value of g_{mc} increases with a decrease in nL. From Equation (1) we know that R_M is inversely proportional to nL, and this explains why a larger g_{mc} is required to start oscillation. On the other hand, if nL is too large, then the impedance of C_0 is low and R_0 becomes a significant part of power loss in the circuit. Therefore, g_{mc} needs to increase with large values of nL, (assuming R_0 stays constant) to compensate for losses in the parasitics. Thus, the effective resonator length, nL, can be optimized for minimum power consumption. The resonator thickness, T, has little effect within this optimal region and therefore any thickness could be employed. To ensure good material quality of the sputter-deposited AlN and low device impedance ($1/j\omega C_0$), we chose T = 2 µm, L = 200 µm, and n = 3, for the 222 MHz resonator.

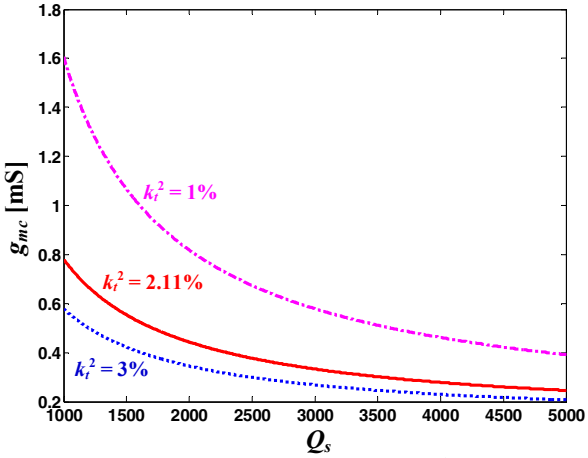

Fig. 5. g_{mc} vs Q_s for different k_t^2

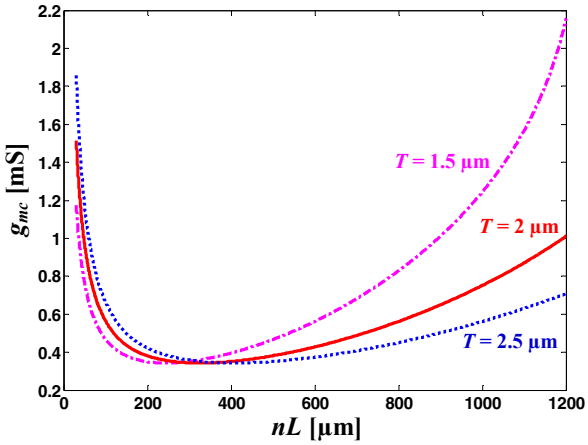

Fig. 6. g_{mc} vs nL for different T

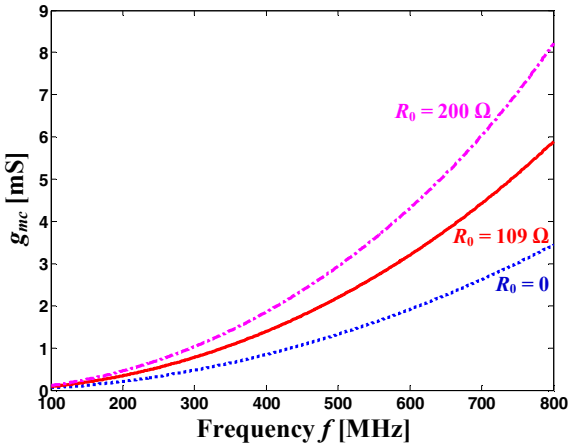

Fig. 7. g_{mc} vs f for different R_0

Finally, in order to demonstrate a single circuit (amplifier) design that works for multi-frequency resonators, we studied g_{mc} as a function of operation frequency f and parasitic resistance R_0 (Fig. 7). As Equation (2) implies, given a certain R_N, g_{mc} rapidly increases with frequency. At high frequencies, the effect of R_0 becomes more pronounced as was already illustrated in Fig. 6 (the impedance associated with C_0 lowers with increasing frequency). By comparing Fig. 5 – 7, we found that the dominating parameter that set the single Pierce circuit design for multi-frequency oscillators was the operation frequency. In this work, we decided to demonstrate oscillators up to 500 MHz. In this case, the minimum g_{mc} required to initiate oscillation was ~2 mS (as shown in Fig. 7). As a rule of thumb, a transconductance g_m larger than two times the minimum g_{mc} is usually needed to ensure oscillations in the circuit. Therefore a g_m of 7.6 mS was chosen for the final design.

Besides, to interface the oscillator circuit with the 50 Ω measurement system, a carefully designed on-chip buffer is added, such that minimum capacitive loading is seen by the oscillator core. We chose a topology that has a PMOS source follower cascaded by a NMOS source follower, which allows a wide range of DC input voltages without the need for an AC coupling capacitor.

IV. Experimental Results

The Pierce oscillator circuit design was implemented in the AMIS 0.5 µm 5 V CMOS process, while the piezoelectric AlN contour-mode resonators were fabricated using a five-mask process as previously described in [4]. The IC chip is currently connected to the MEMS resonator chip by conventional wirebonding (as shown in Fig. 1). Nonetheless, post-CMOS MEMS-IC integration can be envisioned, since these devices are fabricated at very low temperature. Both chips were mounted on a PCB board and the oscillator output voltage was monitored via an Agilent® E5052B Signal Source Analyzer (for phase noise measurement) and an Agilent® MSO6104A Oscilloscope (for time domain measurements). The phase noise measurement results are summarized in Table II. As we

Table II. Experimental results of the Pierce oscillators based on piezoelectric AlN contour-mode resonators.

Oscillator			Resonator				
f_o [MHz]	P_o [dBm]	PN @ 1kHz	f_s [MHz]	Q_s	f_p [MHz]	Q_p	k_t^2
176.12	-4.7	-79 dBc/Hz	175.45	1500	176.54	2000	1.52%
222.49	-4.8	-88 dBc/Hz	221.65	2100	223.56	650	2.11%
306.81	-6.7	-84 dBc/Hz	305.66	1400	307.84	1900	1.75%
482.44	-13.6	-68 dBc/Hz	481.56	850	484.00	1100	1.24%

f_o: oscillation frequency; P_o: oscillator output power; PN: phase noise

can see, multi-frequency (176, 222, 307, and 482 MHz) Pierce oscillators have been demonstrated based on piezoelectric AlN contour-mode MEMS resonators. All the oscillators show phase noise values between –88 and –68 dBc/Hz at 1 kHz offset and phase noise floors as low as –160 dBc/Hz at 1 MHz offset. The same Pierce circuit design is employed to sustain oscillations at the 4 different frequencies, while the oscillator core consumes 10 mW with a 5 V DC supply.

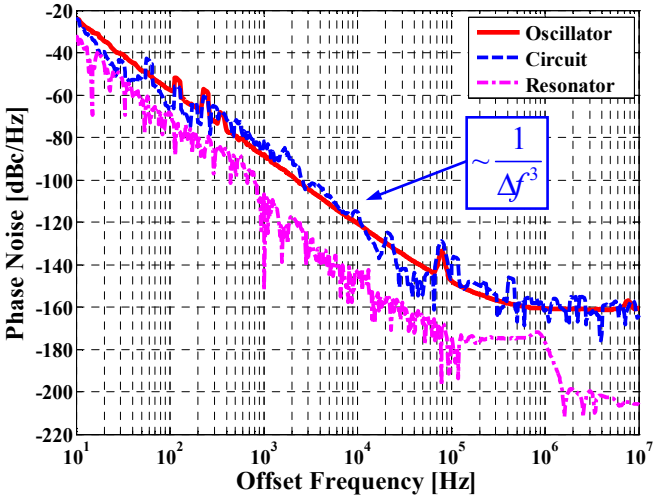

Fig. 8. Closed-loop phase noise plots of the 222 MHz oscillator (continuous red line) and the corresponding contributions from circuit (dotted blue line) and resonator (dotted pink lower line).

In Fig. 8, the measured PN of the 222 MHz oscillator is plotted as a function of the offset frequency, Δf, from the carrier. The curve follows a $\sim 1/\Delta f^3$ trend for offsets within the 10^1 to 10^5 Hz range and has a PN floor of –160 dBc/Hz beyond 10^6 Hz. Generally, oscillator phase noise can be modeled by the following equation [11, 12]:

$$S_{o\phi} = \left(f_o / 2Q_L\Delta f\right)^2 \left[S_{r\phi} + S_{c\phi}\right] + S_{c\phi} = \left(\frac{f_o}{2Q_L\Delta f}\right)^2 \left[\frac{\alpha_{r\phi}}{\Delta f} + \frac{\alpha_{c\phi}}{\Delta f} + \frac{kTFG}{2P_o}\right] + \frac{\alpha_{c\phi}}{\Delta f} + \frac{kTFG}{2P_o} \quad (4)$$

where $S_{o\phi}(\Delta f)$ is the closed-loop phase noise of the oscillator; $S_{r\phi}$ and $S_{c\phi}$ are the open-loop phase noise of the resonator and circuit, respectively; f_o is the oscillation frequency; Q_L is the loaded resonator quality factor; $\alpha_{r\phi}$ and $\alpha_{c\phi}$ are the $1/f$ noise coefficients for the resonator and circuit, respectively; k is the Boltzmann constant; T is the temperature; F and G are the noise figure and power gain of the circuit; P_o is the output power of the oscillator. To analyze the two primary sources (circuit and resonator) of phase noise in the 222 MHz oscillator, the open-loop PN levels of the corresponding circuit and resonator were measured separately. The respective closed-loop PN contributions of the resonator or circuit can be calculated once $S_{c\phi}$ or $S_{r\phi}$ are known. The calculated results are also plotted in Fig. 8 for comparison. As we can see, the circuit PN is higher and matches well with that of the oscillator. Basically the close-to-carrier PN is dominated by the circuit $1/f$ noise, while the far-from-carrier PN floor is determined by the circuit noise figure. Therefore, we conclude that, in this particular design, the CMOS circuit itself, and not the piezoelectric AlN contour-mode resonator, limits the phase noise level of the oscillator. Better PN performances can then be attained if a noise optimization for the circuit is conducted or a lower noise technology is adopted.

V. Discussion

Although in its early stage, oscillator development based on MEMS resonators has received a lot of attention in both academia and industry. Electrostatic transduction mechanism has been most widely used, and representative works can be found in the literature [13 – 15]. Two start-up companies, SiTime® and Discera®, are also geared to provide MEMS oscillators for the replacement of quartz crystals. However, all the demonstrated operating frequencies have been below 125 MHz. Furthermore, electrostatic MEMS resonators are intrinsically associated with high DC polarization voltages, large motional resistance, and vacuum packaging, which constitute a considerable drawback and especially impede the realization of high frequency reference elements. On the other hand, piezoelectric-on-substrate resonator based oscillators have also been demonstrated in [16 – 18]. In this case, the two-port configuration complicates the circuit design. The transducer capacitance is present at the input and output ports of the resonator and constitutes a fundamental problem in achieving high close-loop gain at low power consumption for operation frequencies reaching the GHz range.

Another competing technology operating in the frequency range from 100 MHz to 1 GHz is the SAW-based oscillator. Compared with SAW oscillators, the work demonstrated here provides a 20X reduction in resonator size thanks to piezoelectric AlN contour-mode MEMS technology. Further, the same Pierce CMOS circuit design works for all the multi-frequency oscillators so that a truly single-chip reconfigurable reference solution [5] can be implemented by fabricating AlN RF MEMS resonators and switches [4] on top of the CMOS chip. It can be easily envisioned that chip area, parasitic and power consumption will be reduced to a large extent by this fully integrated solution. Such a solution is very well suited for next-generation reconfigurable and multi-band wireless

communications and sensing [19, 20] applications. Indeed, further developments both at the circuit design and resonator levels need to be made to match the phase noise performance of state-of-the-art SAW oscillators [21].

VI. Conclusion

For the first time, multi-frequency (176, 222, 307, and 482 MHz) Pierce oscillators have been designed, fabricated and tested based on piezoelectric AlN contour-mode MEMS resonators. All oscillators show phase noise (*PN*) values between –88 and –68 dBc/Hz at 1 kHz offset and *PN* floor values as low as –160 dBc/Hz at 1 MHz offset. The same Pierce circuit design is employed to sustain oscillations at the 4 different frequencies, while the oscillator core consumes a low power of 10 mW in the AMIS 0.5 μm 5 V CMOS process. This new piezoelectric AlN contour-mode technology also enables monolithic integration of AlN RF MEMS switch arrays on the same Si substrate. This makes possible a single-chip multi-frequency reconfigurable solution that can be employed in next-generation wireless communications and sensing applications. In future work, we would like to expand this technology to GHz frequency, so that direct frequency synthesis can be achieved for several wireless communication bands.

Acknowledgment

The authors would like to thank Zheng Yang, Viktor Gruev and Rashed Mahameed for their help with the chip design and wirebonding. We would also like to thank the MOSIS Educational Program for the IC chip fabrication and the staff at the Wolf Nanofabrication Facility at Penn for their support in the MEMS fabrication. Finally, AlN deposition has been performed by the Tegal Corporation. The other members of the Penn Micro and Nano Systems Lab also deserve special thanks for their precious discussions and help.

References

[1] C. T.-C. Nguyen, "MEMS technology for timing and frequency control," *IEEE Trans. On Ultrasonics, Ferroelectrics, and Frequency Control*, vol. 54, no. 2, pp. 251-270, Feb 2007.

[2] G. Piazza, P. J. Stephanou, and A. P. Pisano, "Piezoelectric Aluminum Nitride Vibrating Contour-Mode MEMS Resonators", *Journal of MicroElectroMechanical Systems*, vol. 15, no.6, Dec 2006.

[3] G. Piazza, P. J. Stephanou, and A. P. Pisano, "AlN Contour-Mode Vibrating RF MEMS for Next Generation Wireless Communications," *ESSDERC 2006*, Montreux, Switzerland, Sep 2006.

[4] N. Sinha, R. Mahameed, C. Zuo, M. B. Pisani, C. R. Perez, and G. Piazza, "Dual-Beam Actuation of Piezoelectric AlN RF MEMS Switches Monolithically Integrated with AlN Contour-Mode Resonators", *2008 Solid State Sensor, Actuator and Microsystems Workshop (Hilton Head 2008)*, pp. 22-25, South Carolina, USA, 2008.

[5] G. Piazza, P. J. Stephanou, and A. P. Pisano, "One and Two Port Piezoelectric Higher Order Contour-Mode MEMS Resonators for Mechanical Signal Processing", *Solid-State Electronics*, vol. 51, pp. 1596–1608, 2007.

[6] J. D. Larson III, P. D. Bradley, S. Wartenberg, and R. C. Ruby, "Modified Butterworth-Van Dyke Circuit for FBAR Resonators and Automated Measurement System," *2000 IEEE Ultrasonics Symposium*, pp. 863-868, Oct 2000.

[7] W. M. C. Sansen, *Analog Design Essentials*, Springer, 2006.

[8] E. A. Vittoz, M. G. R. Degrauwe, and S. Bitz, "High-Performance Crystal Oscillator Circuits: Theory and Application", *IEEE Journal of Solid-State Circuits*, vol. 23, no. 3, Jun 1988.

[9] J. T. Santos and R. G. Meyer, "A One-Pin Crystal Oscillator for VLSI Circuits", *IEEE Journal of Solid-State Circuits*, vol. sc-19, no. 2, 1984.

[10] C. Zuo, N. Sinha, M. B. Pisani, C. R. Perez, R. Mahameed, and G. Piazza, "Channel-Select RF MEMS Filters Based On Self-Coupled AlN Contour-Mode Piezoelectric Resonators", *2007 IEEE International Ultrasonics Symposium*, New York, USA, Oct 2007.

[11] E. S. Ferre-Pikal, "PM and AM Noise Measurement Techniques – Part I", *2002 IEEE International Frequency Control Symposium Tutorials*.

[12] T. E. Parker, "Characteristics and Sources of Phase Noise in Stable Oscillators", *41st Annual Frequency Control Symposium*, 1987.

[13] Y.-W. Lin, S. Lee, S.-S. Li, Y. Xie, Z. Ren, and C. T.-C. Nguyen, "Series-Resonant VHF Micromechanical Resonator Reference Oscillators", *IEEE J. of Solid-State Circuits*, vol. 39, no. 12, Dec 2004.

[14] V. Kaajakari, P. Rantakari, J. K. Koskinen, T. Mattila, J. Kiihamaki, M. Koskenvuori, I. Tittonen, and A. Oja, "Low Noise Silicon Micromechanical Bulk Acoustic Wave Oscillator", *2005 IEEE Ultrasonics Symposium*, Rotterdam, The Netherlands, Sep 2005.

[15] W.-L. Huang, Z. Ren, Y.-W. Lin, H.-Y. Chen, J. Lahann, and C. T.-C. Nguyen, "Fully monolithic CMOS nickel micromechanical resonator oscillator," *IEEE MEMS 2008 Conference*, Tucson, Arizona, pp. 10-13, Jan 2008,

[16] H. M. Lavasani, R. Abdolvand, and F. Ayazi, "A 500MHz Low Phase-Noise AlN-on-Silicon Reference Oscillator", *2007 IEEE Custom Integrated Circuits Conference*.

[17] R. Abdolvand, H. Mirilavasani, and F. Ayazi, "Single-Resonator Dual-Frequency Thin-Film Piezoelectric-on-Substrate Oscillator", *2007 IEEE International Electron Devices Meeting*.

[18] H. M. Lavasani, R. Abdolvand, and F. Ayazi, "Low Phase-Noise UHF Thin-Film Piezoelectric-On-Substrate LBAR Oscillators", *IEEE MEMS 2008 Conference*, Tucson, Arizona, Jan 2008.

[19] M. Rinaldi, C. Zuniga, N. Sinha, M. Taheri, S. M. Khamis, A. T. Johnson and G. Piazza, "Gravimetric Chemical Sensor Based on the Direct Integration of SWNT's on AlN Contour Mode MEMS Resonators", *2008 IEEE International Frequency Control Symposium*.

[20] E. Zampetti, S. Pantalei, A. Macagnanoa, E. Proietti, C. Di Natale, A. D'Amico, "Use of a Multiplexed Oscillator in a Miniaturized Electronic Nose based on a Multichannel Quartz Crystal Microbalance", *Sensors and Actuators B*, vol. 131, pp. 159–166, 2008.

[21] G. K. Montress, T. E. Parker, and D. Andrea, "Review of SAW Oscillator Performance", *1994 IEEE Ultrasonics Symposium*, vol. 1, pp. 43-54, 1994.